The Journal of Experimental Biology 207, 4393-4405
Published by The Company of Biologists 2004
doi:10.1242/jeb.01318

Crater landscape: two-dimensional oxygen gradients in the circulatory system of the microcrustacean *Daphnia magna*

R. Pirow*,†, C. Bäumer† and R. J. Paul

Institut für Zoophysiologie, Westfälische Wilhelms-Universität, Hindenburgplatz 55, 48143 Münster, Germany

*Author for correspondence (e-mail: pirow@uni-muenster.de)

†These authors contributed equally to this work

Accepted 29 September 2004

Summary

Oxygen transport processes in millimetre-sized animals can be very complex, because oxygen molecules do not exclusively follow the pathway predetermined by the circulating fluid but may also simultaneously move from the respiratory surfaces to the tissues along different paths by diffusion. The present study made use of the oxygen-sensitive phosphorescence probe Oxyphor R2 to analyze the internal oxygen pathway in the transparent microcrustacean *Daphnia magna*. Oxyphor R2 was injected into the circulatory system and the distribution of oxygen partial pressure (P_{O_2}) in the haemolymph was measured by phosphorescence lifetime imaging in the P_{O_2} range 0–6 kPa (0–30% air saturation). There were substantial differences in the shape of the two-dimensional P_{O_2} profiles depending on the concentration of haemoglobin (Hb) in the haemolymph. A steep global gradient, from posterior to anterior, occurred in animals with low concentrations of Hb (90–167 μmol l^{-1} haem). In contrast, animals with a five- to sixfold higher concentration of Hb showed flat internal P_{O_2} gradients which, however, were only present under reduced ambient oxygen tensions ($P_{O_{2amb}}$=3–1 kPa), when Hb was maximally involved in oxygen transport. Under these conditions, the presence of Hb at high concentrations stabilized the unloading P_{O_2} in the central body to 0.9–0.4 kPa. Independent of Hb concentration and body size, the loading P_{O_2} was always 0.5 kPa below the $P_{O_{2amb}}$. From these P_{O_2} profiles, it was possible (i) to follow the track of oxygen within the animal, and (ii) to visualize the shift from a diffusion-dominated to a convection-dominated transport as a result of increased Hb concentration.

Key words: Crustacea, Branchiopoda, Cladocera, *Daphnia*, zooplankton, oxygen transport, ventilation, circulatory system, diffusion, convection, haemoglobin, hypoxia, phosphorescence lifetime imaging.

Introduction

Diffusion and convection are the two mechanisms by which aerobic animals maintain a continuous flow of oxygen from the environment to their tissues (Weibel, 1984). The term convection refers to the transfer of oxygen in a mass of air or liquid (e.g. water or blood) by the movement of that mass. Diffusion is the process whereby oxygen and other molecules of liquids or gases intermingle as the result of their random thermal motion. Although molecular motion occurs randomly in all spatial directions, an uneven distribution of oxygen molecules, e.g. across the respiratory surface or within a mass of tissue, results in a directional net diffusion of those molecules from a region of higher partial pressure to one of lower partial pressure.

Diffusion is effective for short distances only, so its relevance is usually restricted to transport processes across thin physical barriers such as the respiratory surfaces and within the tissues. Convection, in contrast, often dominates the transport of oxygen in moving respiratory media and circulating body fluids. Ventilatory and circulatory convection serve to bridge long transport distances that may exist between the ambient medium and the respiratory surfaces and between the respiratory surfaces and the tissues. The mutually exclusive dominance of diffusion and convection within the individual steps of the oxygen transport cascade has made it possible to describe oxygen transport in large, physiologically advanced animals by straightforward mathematical relationships (Piiper, 1982; Weibel, 1984; Shelton, 1992) with only a few parameters and variables, which are accessible by morphometric techniques (e.g. Weibel, 1979, 1980) and classical physiological methods.

This concept of oxygen transport, however, appears to be too simple when body sizes shrink to the millimetre scale. In these tiny organisms, transport of oxygen from the respiratory surfaces to the tissues does not exclusively follow the pathway predetermined by the circulating fluid. In addition, oxygen may be moved simultaneously to the target tissues along different paths by diffusion. The increasing influence of diffusion therefore complicates the mathematical description of

circulatory oxygen transport. Moreover, small body size is an experimental obstacle that hampers attempts to obtain adequate physiological information. Fortunately, recent advances in optical techniques and digital image processing have expanded the methodical versatility of microscopy, so that this information can be obtained in animals that are highly transparent (Colmorgen and Paul, 1995; Burggren and Fritsche, 1995; Paul et al., 1997, 1998; Schwerte and Fritsche, 2003).

The transparent microcrustacean *Daphnia magna* (Branchiopoda, Cladocera) is a valuable model organism that has stimulated the development and adaptation of innovative optical techniques for studying oxygen transport processes in millimetre-sized animals. These methods have made it possible to obtain information on physiological key parameters such as ventilation and perfusion rates, the *in vivo* oxygen saturation of haemoglobin, oxygen partial pressure and tissue oxygenation state (Paul et al., 1997; Pirow et al., 1999a,b, 2001; Bäumer, 2001; Bäumer et al., 2002; Seidl et al., 2002). The availability of physiological information has initiated attempts to push conceptual barriers and to make use of the increasing computational power for modelling and simulation of oxygen transport in millimetre-sized animals (Pirow, 2003; Pirow and Buchen, 2004).

These *in vivo* and *in silico* approaches were largely motivated by the intention to comprehend the physiological implications of the presence of haemoglobin (Hb) in *D. magna*. In contrast to other crustaceans, which use haemocyanin as the respiratory protein, branchiopod crustaceans including *D. magna* have a Hb that is freely dissolved in the haemolymph (e.g. Weber and Vinogradov, 2001). When challenged by a reduction in ambient oxygen partial pressure (P_{O2amb}), *D. magna* shows a striking increase in Hb concentration (e.g. Kobayashi and Hoshi, 1982; Zeis et al., 2003a,b). The rise in concentration is accompanied by an increase in oxygen affinity (e.g. Kobayashi et al., 1988) resulting from an altered subunit composition of the multimeric protein (e.g. Kimura et al., 1999; Zeis et al., 2003a,b).

Variations in the concentration and oxygen affinity of Hb should affect the gradients of oxygen partial pressure (P_{O_2}) in the circulatory system, causing alterations in the relative contributions of convection and diffusion to circulatory oxygen transport. So far, nothing is known about the internal oxygen milieu except some indirect information from studies on the *in vivo* oxygenation state of Hb (Hoshi and Yahagi, 1975; Kobayashi and Tanaka, 1991; Pirow et al., 1999b, 2001). Direct measurement of the internal P_{O_2} would facilitate elucidation of the effect of Hb on circulatory oxygen transport. In providing information about the *in vivo* P_{O_2} experienced by the tissues, such measurements would also be of interest for studies on oxygen-dependent gene expression. Finally, we would be able to learn more about the homeostatic abilities of an animal whose internal milieu, owing to its small body size, is much more affected by environmental disturbances than that of larger animals.

In the present study, we therefore analysed the internal oxygen distribution in different sized Hb-poor and Hb-rich animals of *D. magna* under varying ambient oxygen conditions. To profile the P_{O_2} in the circulatory system, we made use of an oxygen-sensitive phosphorescence probe introduced into the circulatory system by microinjection. The method employed is based on the oxygen-dependent quenching of phosphorescence and has the great advantage that it is non-invasive, except for the addition of the phosphorence probe, and its calibration is absolute (Dunphy et al., 2002).

Materials and methods

Animals

Female water fleas *Daphnia magna* Straus were initially obtained from the Staatliches Umweltamt, Münster, Nordrhein-Westfalen, Germany and have been kept in laboratory culture under normal and reduced oxygen conditions (normoxia, hypoxia) at room temperature (20–22°C) for at least half a year. The two oxygen conditions resulted in animals of different acclimatory states with different concentrations of Hb in the haemolymph. Normoxia-acclimated, Hb-poor animals were kept in groups of 25–50 individuals in 1–2 l glass beakers filled with air-saturated medium (M4 medium; Elendt and Bias, 1990). Hypoxia-acclimated, Hb-rich animals were kept in batches of 40–50 individuals in 3–4 l preserving jars filled with 1.5–2 l oxygen-poor medium. The low oxygen concentration resulted from reduction of the atmospheric pressure in the residual air space of the preserving jar to one tenth of the standard atmospheric pressure at sea level. To boost the formation of Hb under hypoxic conditions, ferrous sulphate ($FeSO_4 \cdot H_2O$) was added to the medium at a final concentration of 396 mg l^{-1} every second week. Hb-poor animals were reared under a 16 h:8 h L:D photoperiod using daylight fluorescent lamps, whereas Hb-rich animals were kept under continuous, dimmed light conditions to minimize the production of oxygen *via* photosynthesis of the food algae. Both groups of animals were fed with yeast and algae (*Desmodesmus subspicatus*) once daily.

For the experiments, the animals were separated into three size groups (small, medium, large) according to their body length (*BL*), which was measured from the base of the posterior apical spine to the head. Small, medium and large Hb-poor animals had *BL*=1.4–1.7 mm (1.5±0.1 mm, *N*=6; means ± S.D.), 2.5–2.7 mm (2.6±0.1 mm, *N*=4) and 3.1–3.5 (3.3±0.1 mm, *N*=6). Hb-rich animals were generally smaller than Hb-poor animals as a consequence of hypoxic incubation (Kobayashi, 1982), so only small and medium-sized animals with *BL*=1.4–1.8 mm (1.6±0.1 mm, *N*=5) and 2.6–2.9 mm (2.7±0.1 mm, *N*=7) were studied. Those animals that had already attained sexual maturity (i.e. the medium and large-sized animals) had at most ten parthenogenetic embryos of developmental stages 1–4 (see table 3 of Green, 1956) in the brood chamber.

The oxygen-sensitive phosphorescence probe

The oxygen-sensitive probe Oxyphor R2, a polyglutamic dendrimer containing Pd-meso-tetra-(4-carboxyphenyl)porphyrin (Dunphy et al., 2002), purchased from Oxygen Enterprises (Philadelphia, PA, USA). Oxyphor R2, of molecular mass of 2794 Da, possesses two absorption maxima at 415 and 524 nm and shows a phosphorescence emission near 700 nm. The extinction coefficient at 524 nm is 19 mmol l^{-1} cm^{-1} and the quantum efficiency of phosphorescence is approximately 10% (Dunphy et al., 2002).

The method for measuring oxygen is based on the suppression of phosphorescence by molecular oxygen (Vanderkooi and Wilson, 1986). When excited by light, the probe molecules enter into the triplet state. The phosphorescence arises when the excited triplet state molecule returns to the ground state with emission of a photon. In the presence of molecular oxygen, the excited molecules may transfer their energy to oxygen and return to the ground state without phosphorescence emission.

Because the rate of decay of the triplet state is proportional to the concentration of excited triplet state molecules, which in turn is proportional to phosphorescence intensity (I_t), the decay of I_t after an excitation flash given at time t=0 follows an exponential law (Vinogradov and Wilson, 1994):

$$I_t = I_0 e^{-t/\tau} , \quad (1)$$

where τ (s) is the phosphorescence lifetime, and I_0 is the initial light intensity immediately after the excitation flash. τ depends on oxygen concentration, and this dependency is described by the Stern–Volmer equation:

$$1/\tau = 1/\tau_0 + k_q P_{O_2} , \quad (2)$$

where τ_0 (s) is the lifetime at zero-oxygen concentration, k_q (kPa^{-1} s^{-1}) is the quenching constant, and P_{O_2} (kPa) is the oxygen partial pressure (Vinogradov and Wilson, 1994). k_q is a second order rate constant related to the frequency of collisions between the triplet state probe molecules and molecular oxygen.

Microscopic arrangement for the optical measurement of P_{O_2}

The phosphorescence imaging system consisted of an inverted microscope (Zeiss Axiovert 100, Carl Zeiss, Oberkochen, Germany) equipped with a pulsed Xenon microsecond flashlamp (μF900; Edinburgh Analytical Instruments, Edinburgh, UK) for phosphorescence excitation (Fig. 1). The flashlamp produced flashes of 3 μs duration (full width at half-maximum pulse height) at a rate of 100 Hz. The reflector slider of the microscope contained a bandpass excitation filter with a transmittance wavelength of 535±35 nm (peak wavelength ± full width at half-maximum transmission bandwidth), a dichroic mirror with a cut-off wavelength of 580 nm and a long-pass emission filter with cut-off wavelength of 590 nm. The phosphorescence of the oxygen probe was imaged by a 16-bit liquid-nitrogen-cooled slow-scan CCD camera (576×384 pixels; LN/CCD-576E, Princeton Instruments, Trenton, NJ, USA), which was coupled to a gatable image intensifier (Princeton Instruments). Gate pulses and high voltage were provided to the intensifier by a programmable pulse gate generator (PG200 with MCP-100 option; Princeton Instruments). Two computers served to control the activity of all system components and synchronized image acquisition with phosphorescence excitation and gating of the image intensifier.

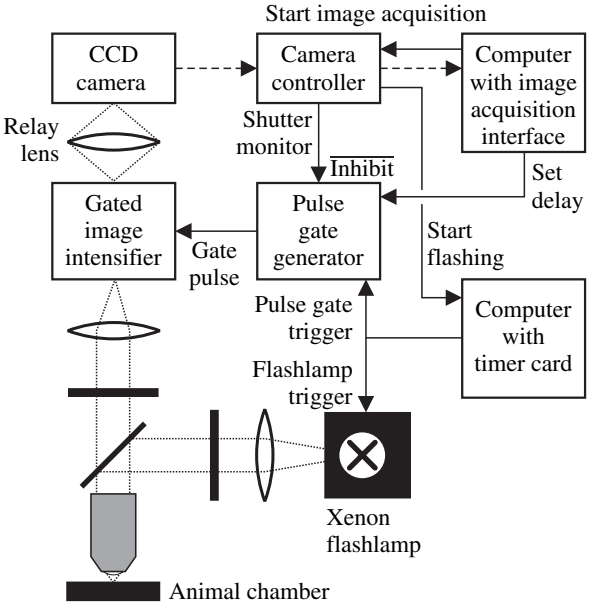

Fig. 1. Schematic diagram of the microscopic set-up used for P_{O_2} imaging, showing the major components, the light path (dotted lines) and the pathways for image data (broken arrows) and signal data (solid arrows).

For image acquisition, we used the imaging software WinView 1.6.1.1 (Princeton Instruments), whose built-in Macro language made it possible to automate image-acquisition sequences and to control the activities of all system components. The acquired images had a reduced resolution of 288×192 pixels resulting from a hardware binning of 2×2 pixels. Before analysis, images were smoothed by a 3×3 low pass filter to remove random noise.

To monitor the circulatory activity of the animal during the experiments, the heart rate was determined (Paul et al., 1997) in parallel to P_{O_2} by trans-illuminating the animal with infrared light (λ>830 nm). To avoid optical interferences on the P_{O_2} measurement, the infrared illumination was blocked by a mechanical shutter during the acquisition of phosphorescence images.

Collection of phosphorescence intensity images

Image acquisition followed the procedure developed by Pawlowski and Wilson (1994). To collect a single phosphorescence intensity image, the imaging system triggered the flashlamp at t=0 to excite the probe molecules. After waiting a certain delay time t_d (s), the image intensifier was turned on to integrate the phosphorescence light emitted during the time interval from t=t_d to t=t_d+ΔT, where ΔT

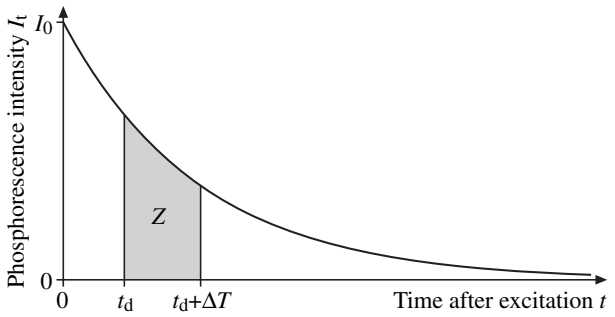

Fig. 2. Timing of phosphorescence image acquisition. The curve shows the exponential decay of phosphorescence intensity I_t after an excitation flash at time t=0. The image intensifier is turned on at delay time t_d for the gate period ΔT. The grey-shaded area indicates that portion of phosphorescence light (Z) that is integrated on the CCD array during ΔT. I_0, initial phosphorescence intensity immediately after the excitation flash.

(=240 μs) is the gating pulse duration (Fig. 2). Depending on signal intensity, the flash lamp was triggered 800–1600 times at 10 ms intervals (with appropriate gating of the intensifier at a given t_d) while the CCD camera integrated the collected phosphorescence light from the flash sequence in a single exposure.

To follow the exponential decay of phosphorescence intensity, a set of phosphorescence intensity images was taken at seven different t_d (10, 20, 40, 80, 160, 300, 600 μs; Fig. 3). From these images, a background image taken at t_d=3000 μs was subtracted to remove the influence of light arising from non-phosphorescence sources. The collection of eight phosphorescence intensity images, required to obtain a single P_{O_2} image, took 2–4 min depending on the number of excitation flashes (800 or 1600) per phosphorescence intensity image.

Calculation of phosphorescence lifetime and oxygen partial pressure

A set of phosphorescence intensity images can be regarded as a three-dimensional data package of intensity values $Z(x,y,t_d)$ comprising the integrated intensity (Z) for each pixel coordinate (x,y) as a function of delay time t_d (Fig. 3). For each pixel coordinate, a single-exponential decay was fitted to the data $Z(t_d)$ based on the following equation (Pawlowski and Wilson, 1994):

$$Z(t_d) = \int_{t_d}^{t_d+\Delta T} I_t \mathrm{d}t = \int_{t_d}^{t_d+\Delta T} I_0 e^{-t/\tau} \mathrm{d}t = (1-e^{-\Delta T/\tau}) I_0 \tau e^{-t_d/\tau} . \quad (3)$$

This equation was linearized by taking the logarithms of both sides and a linear regression analysis then yielded the phosphorescence lifetime τ and the initial phosphorescence intensity I_0 immediately after the excitation flash. Information on τ was employed to calculated the P_{O_2} according to Equation 2 on the basis of the calibration parameters τ_0 and k_q. A pixel coordinate was regarded to contain valid information on P_{O_2}, when the following conditions were fulfilled. (1) The intensity value Z at t_d=10 μs exceeded a threshold intensity measured at the boundary of the object containing the oxygen-sensitive dye. (2) The squared correlation coefficient r^2 was greater than 0.95. (3) The phosphorescence lifetime τ was within the range of 0–700 μs. (4) The P_{O_2} was lower than P_{O_2amb}+0.7 kPa.

After analyzing the intensity decay curves at all x,y positions, the results were depicted in an image in which pixel intensity encoded the P_{O_2} in pseudo-colour presentation (Fig. 4). For those x,y coordinates where the four plausibility criteria were not met, the pixel position was masked out by setting pixel intensity to black colour. The P_{O_2} analysis was performed by a program module written in Microsoft Visual

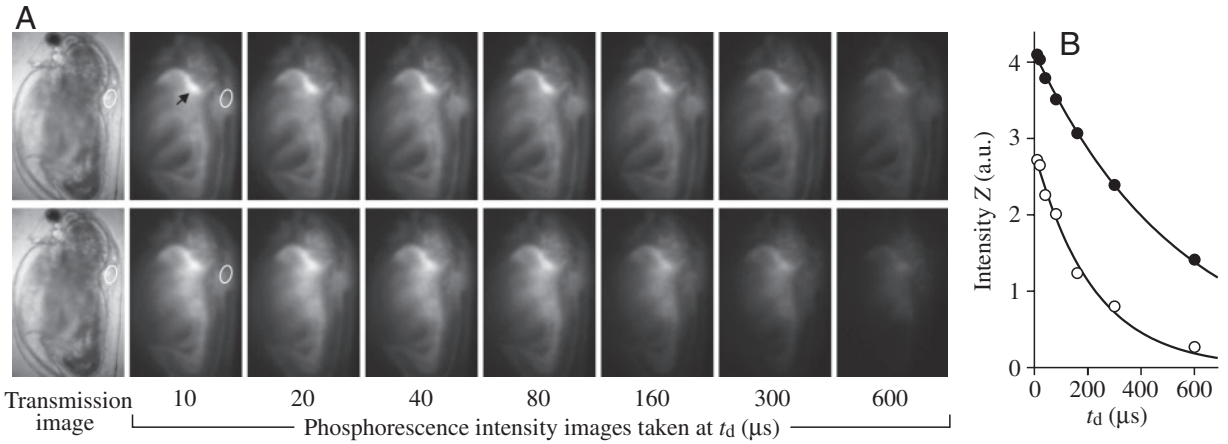

Fig. 3. (A) Sets of phosphorescence intensity images of a 1.4 mm Hb-poor *Daphnia magna* taken at seven different delay times (t_d) under 0.5% (top) and 19.6% air saturation (bottom), respectively. From all phosphorescence images, a background image acquired at t_d=3000 μs has been subtracted. For orientation, an image of the animal taken under transmission illumination is shown at the left. In the top sequence, the limbs appear in sharp contours because the animal had stopped its limb beating activity owing to the low oxygen conditions. Note the strong phosphorescence signal in the region of the shell gland (arrow). (B) For the heart region, i.e. the image areas marked by white ellipses in A, the integrated phosphorescence intensity (Z) was plotted against t_d. Exponential decay curves (solid lines) were fitted according to Equation 3 to the data that were measured at 0.5% (filled circles) and 19.6% air saturation (open circles). a.u., arbitrary units.

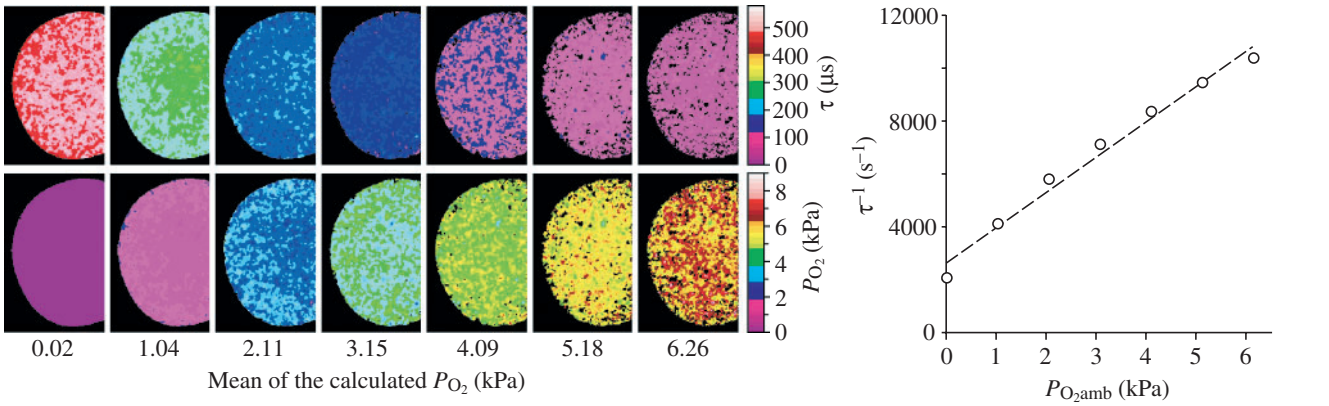

Fig. 4. Example of a calibration experiment of Oxyphor R2 in the haemolymph of a Hb-poor *Daphnia magna*. A circular drop of the dye-loaded haemolymph sample was equilibrated at seven different ambient oxygen tensions (P_{O2amb}=0, 1.02, 2.05, 3.07, 4.09, 5.12, 6.14 kPa; 0–30% air saturation). The phosphorescence lifetime (τ) of the sample was imaged and is depicted in pseudo-colour presentation (top row). Pixel positions outside the sample image were masked out by setting pixel intensity to black colour. The relationship between the reciprocal of the mean τ of each image and P_{O2amb} (open circles) was then analyzed by linear regression analysis using the Stern–Volmer equation ($\tau^{-1}=\tau_0^{-1}+k_qP_{O2amb}$), which yielded the estimates of the lifetime at zero-oxygen concentration (τ_0) and of the quenching constant (k_q). τ_0 and k_q were used to transform phosphorescence lifetime images (top row) into oxygen partial pressure (P_{O_2}) images (bottom row). The numbers below the gallery indicate the mean value of each P_{O_2} image.

C++, which made use of the functionality of the imaging software WinView/32 (Princeton Instruments).

Calibration of Oxyphor R2 in the haemolymph

Oxyphor R2 was dissolved in 60 mmol l^{-1} NaCl in a concentration of 10 mg ml^{-1} (i.e. 3.6 mmol l^{-1}). The dissolved phosphorescence probe was 1:10 diluted with buffered saline (60 mmol l^{-1} NaCl, 20 mmol l^{-1} Hepes, pH 7.4 at 20°C) containing 6% bovine serum albumin to obtain a stock solution for injection. The albumin was required for establishing a stable microenvironment for the phosphorescence probe (Lo et al., 1997). To avoid blocking the micropipettes, the stock solution was sterile filtered using cellulose acetate membrane filters (pore size 0.45 µm; Nalgene, Rochester, New York, USA).

The stock solution of the dye was injected in Hb-poor and Hb-rich individuals of *BL* 2.5–3.0 mm. After a 30 s period, which was sufficient time to distribute the dye solution in the circulatory system, one of the large antennae was cut off and the oozing haemolymph aspirated by a pulled glass capillary. The haemolymph sample was then transferred to a coverslip and covered by a layer of silicone oil (Wacker Siliconoel, AK350, Drawin Vertriebs-GmbH, Ottobrunn, Germany) to avoid dehydration. The coverslip was then transferred into a thermostatted perfusion chamber (Paul et al., 1997), where the sample was equilibrated with humidified, normocapnic gas mixtures of different oxygen levels (0–30% air saturation; Fig. 4) using a gas mixing-pump (Wösthoff, Bochum, Germany). The equilibration time per oxygen step was 30–45 min. The phosphorescence lifetime τ was determined at the end of each equilibration step. The relationship between τ and the oxygen partial pressure was then analyzed by linear regression analysis to obtain estimates of the lifetime at zero-oxygen concentration τ_0 and of the quenching constant k_q (Equation 2; Fig. 4).

Microinjection and experimental conditions

Before the start of experiments, animals were transferred into nutrient-free normoxic medium for 1–4 h. The selection of fasting animals ensured that digestive processes did not affect oxygen consumption rate and systemic functions involved in oxygen transport (Pirow and Buchen, 2004). Single animals were immobilized by gluing (with histoacryl; B. Braun AG, Melsungen, Germany) their posterior apical spine to a bristle that was then fixed to a cover glass using a small lump of plasticine.

The oxygen-sensitive dye was introduced into the circulatory system using micropipettes pulled (Puller 88; from Zaschka, Zoologisches Institut, Universität München, Germany) from standard borosilicate glass capillaries (1B100F-4; World Precision Instruments, Sarasota, FL, USA) and bevelled (Beveler 1300M; World Precision Instruments) to an angle of 30°, o.d. 12–26 µm, using a 0.3 µm aluminium oxide-coated film (3 M, Neuss, Germany).

Depending on the animal's body size, a volume of 65–200 nl of a dye stock solution was microinjected (Transjector 5246; Eppendorf, Hamburg, Germany) into the haemolymph space at a dorsal position directly downstream of the heart. The injection volume was chosen to obtain a sufficiently high phosphorescence signal without affecting the rhythmicity of the heart and the limbs. After microinjection, the animal fixed to the cover glass was transferred into a thermostatted perfusion chamber with its head orientated against the medium flow. The large antennae were freely moveable, and the animal did not contact the top and the bottom (cover glass) of the chamber. The flow rate of the medium was set to 8 ml min^{-1}. The chamber was initially perfused with air-saturated medium,

and the animal was allowed to acclimate to these conditions for 30 min.

An adequate phosphorescence signal that allowed the imaging of internal P_{O_2} could only be obtained under hypoxic conditions, because the phosphorescence intensity as well as the change in phosphorescence lifetime per unit change of P_{O_2} decreased with increasing P_{O_2}. Images of internal P_{O_2} were therefore taken at ambient oxygen levels of 30, 25, 20, 16, 12, 10, 8, 4, 2 and 0% air saturation. Each animal was exposed to the descending order of oxygen levels with a duration of 15 min for the first level and of 5 min for all other levels. At the end of each oxygen step, phosphorescence images were taken and the heart rate was measured.

Determination of haemolymph Hb concentration

Haemolymph samples were taken from Hb-poor and Hb-rich individuals of the three different size groups, and Hb concentrations were measured according to Becher (2002). For the small-sized group, haemolymph samples of two individuals with *BL*=1.8–2.0 mm (Hb-poor: 1.9±0.1 mm, *N*=5; Hb-rich: 1.9±0.1 mm, *N*=6) were pooled to obtain a sufficiently large volume for the measurement. It was not possible to examine individuals smaller than 1.8 mm. The medium and large Hb-poor animals had *BL*=2.6±0.1 mm (*N*=6) and 3.5±0.2 mm (N=5), respectively, and the medium Hb-rich animals had *BL*=2.7±0.1 (*N*=5).

To draw a haemolymph sample, the animal was transferred to a microscope slide and adhering water was gently removed with filter paper. Using a very fine spring scissor (No. 15001-08; Fine Science Tools, North Vancouver, Canada), the second antenna was proximally amputated (Fritzsche, 1917) and the oozing haemolymph was aspirated into a 2 µl capillary (minicaps; Hirschmann Laborgeräte, Eberstadt, Germany). The capillary was then transferred into the light path of a monolithic miniature spectrometer (MMS-UV/VIS, spectral range: 194–738 nm, 256 pixel photodiode array; Carl Zeiss OEM-Spektralsensorik, Oberkochen, Germany) coupled *via* a Front End Electronics and a PC interface board (14-bit resolution; tec5 AG, Oberursel, Germany) to a computer. The software SDAS_32D (tec5 AG) was used for spectrum acquisition. Absorption spectra in the range of 520–590 nm were measured under oxygenated conditions using water as reference sample. The haem-based Hb concentration was determined as described elsewhere (Pirow et al., 2001). An appropriate correction for the path length when using a cylindrical capillary as microcuvette was taken into consideration (Becher, 2002).

Statistical analysis

Data were expressed as mean values ± standard deviation (S.D.); *N* = number of animals examined. Statistical differences in mean values were assessed using the *t*-test after differences in variance had been checked using the *F*-test. A two-way ANOVA (Zar, 1999) was applied to test the effect of acclimation state and body size on a physiological variable. Statistical differences were considered significant at $P<0.05$.

Results

Calibration of Oxyphor R2 in the haemolymph

Calibration of the oxygen-sensitive dye was performed from 0% to 30% air saturation (P_{O2amb}=6 kPa). We first checked whether differences in Hb concentration affected the dependency of measured phosphorescence lifetime (τ) on P_{O2amb}. There was no significant difference in the experimentally determined τ at 0 kPa between Hb-poor and Hb-rich haemolymph (470±20 *vs* 459±13 µs; *N*=3 each; *t*-test: *t*=0.80, d.f.=4, *P*=0.47). Plotting the reciprocal of measured phosphorescence lifetime (τ^{-1}) against P_{O2amb} (Fig. 5A) revealed a close linear relationship (r^2>0.999) for Hb-rich haemolymph in the range of 0–6 kPa; for Hb-poor haemolymph, τ^{-1} increased linearly with P_{O2amb} in the range 0–4 kPa but deviated at higher P_{O2amb} from the extrapolated linear relationship. A linear regression analysis of each calibration was therefore performed in the range 0–6 kPa (Hb-rich haemolymph) and 0–4 kPa (Hb-poor haemolymph), respectively, to obtain estimates for lifetime at zero-oxygen tension (τ_0) and quenching constant (k_q) of Equation 2. Both

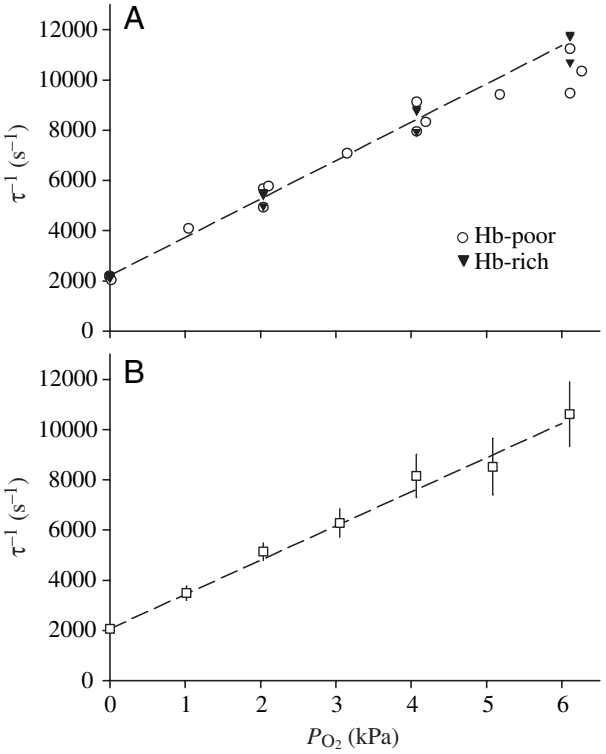

Fig. 5. Calibration of Oxyphor R2 in the haemolymph of *D. magna*. The data show the reciprocal of the phosphorescence lifetime τ plotted against oxygen partial pressure P_{O_2}. (A) Comparison of individual calibrations in Hb-poor (open circles, *N*=3) and Hb-rich haemolymph (filled triangles, *N*=3). Individual calibrations were analyzed by linear regression analysis using the Stern–Volmer equation (Equation 2) and the regression parameters averaged to obtain a mean regression line (broken line). (B) Pooled data (means ± S.D., *N*=7) of further calibrations with Hb-poor and Hb-rich haemolymph. The linear regression line (broken line) was used to convert *in vivo* phosphorescence lifetime images into P_{O_2} images.

k_q (1535±147 *vs* 1519±94 kPa^{-1} s^{-1}; N=3 each; t-test: t=0.17, d.f.=4, P=0.87) and τ_0 (453±20 *vs* 451±20 μs; N=3 each; t-test: t=0.12, d.f.=4, P=0.91) were essentially the same for Hb-poor and Hb-rich haemolymph (mean k_q=1527±111 kPa^{-1} s^{-1}, mean τ_0=452±18 μs).

Further calibrations with Hb-poor and Hb-rich haemolymph (N=7 each) were carried out during the *in vivo* P_{O_2} measurements (Fig. 5B). As in the first calibration experiment (Fig. 5A), we did not find any significant differences (t-test: P>0.44 for all cases) in the experimentally determined τ at 0 kPa (482±32 *vs* 486±35 μs) nor in the derived regression parameters τ_0 (474±50 *vs* 457±19 μs) and k_q (1441±213 *vs* 1457±174 kPa^{-1} s^{-1}) between Hb-poor (P_{O_2amb} range: 0–4 kPa) and Hb-rich haemolymph (P_{O_2amb} range: 0–6 kPa). From these individual calibration data, a mean calibration curve (Fig. 5B) was calculated for the whole P_{O_2amb} range of 0–6 kPa. The derived regression parameters of τ_0=484 μs and k_q=1364 kPa^{-1} s^{-1} were used to convert the *in vivo* phosphorescence lifetime images of all animals into P_{O_2} images. Since the variability of τ increased with increasing P_{O_2amb} (Fig. 5B), P_{O_2} determination was more affected by error at higher than at lower P_{O_2amb} values. For example, at P_{O_2amb} of 6.1 kPa, the individual τ calibration values ranged from 83 to 133 μs (mean=96 μs), which would yield calculated P_{O_2} values of 4.0–7.4 kPa (mean=6.3 kPa). At the lower P_{O_2amb} of 2.0 kPa, individual τ values of 178–231 μs (mean=195 μs) would translate into P_{O_2} values of 1.7–2.6 kPa (mean=2.3 kPa).

Two-dimensional distribution of oxygen partial pressure in the haemolymph

Images showing the P_{O_2} distribution within the circulatory system were obtained from lateral views of the animals. The optical focus was always set in a manner to obtain a sharp image of the heart wall. The phosphorescence signal therefore came predominantly from the animal's median plane and included information from the different haemolymph spaces (lacunae) of the trunk and the limbs, the parts of the carapace lacuna at ventral, posterior and dorsal positions, and the haemolymph space in the head region. Depending on body size, either the whole animal or the dorsal body region only was imaged. A total acquisition time of 2–4 min was needed to obtain the data for one single P_{O_2} image. As a consequence of this long acquisition time, sharp contours of moving structures such as the limbs disappeared in the phosphorescence intensity images (Fig. 3) and, consequently, in the P_{O_2} images (Fig. 6).

Owing to the large haemolymph volume, which in *D. magna* comprises about 60% of total body volume (Kobayashi, 1983), more or less the whole image of the animal contained valid information on P_{O_2} (Fig. 6). The extent of valid P_{O_2} information was lower at higher ambient oxygen partial pressures owing to the reduced phosphorescence intensity.

Inspection of data obtained from small animals (1.5±0.12 mm long) revealed large internal P_{O_2} gradients in Hb-poor and Hb-rich animals at P_{O_2amb}=6.1–6.3 kPa (30% air saturation; Fig. 6). The highest P_{O_2} values mainly occurred in the posterior and dorsal regions of the animals. In Hb-rich animals, high P_{O_2} values extended into the head region including the rostral region. The lowest values were found in the central part of the animals. In Hb-poor animals, this low-oxygen zone was shifted anteriorly. The lowest values occurred in the centre of the anterior half of the animals around the bases of the second antennae.

Lowering the P_{O_2amb} from 6.1 to 1.7 kPa resulted in a flattening of internal P_{O_2} gradients in Hb-rich animals (Fig. 6). These flat profiles contrasted with the steep profiles observed in Hb-poor animals at higher P_{O_2amb} (Fig. 7). In both groups, further reductions of P_{O_2amb} resulted in the formation of anoxic zones, which extended progressively from the central body region to the periphery (Fig. 6). The critical P_{O_2amb} resulting in the incipient formation of anoxic zones was higher in Hb-poor than in Hb-rich animals.

Heart rate

Heart rate (f_H) was monitored in parallel to haemolymph P_{O_2} as an indicator of circulatory activity during the hypoxic exposure experiments, and to assess the influence of the injection procedure on the physiological state of the animals, by comparing the data of our injected animals with those of

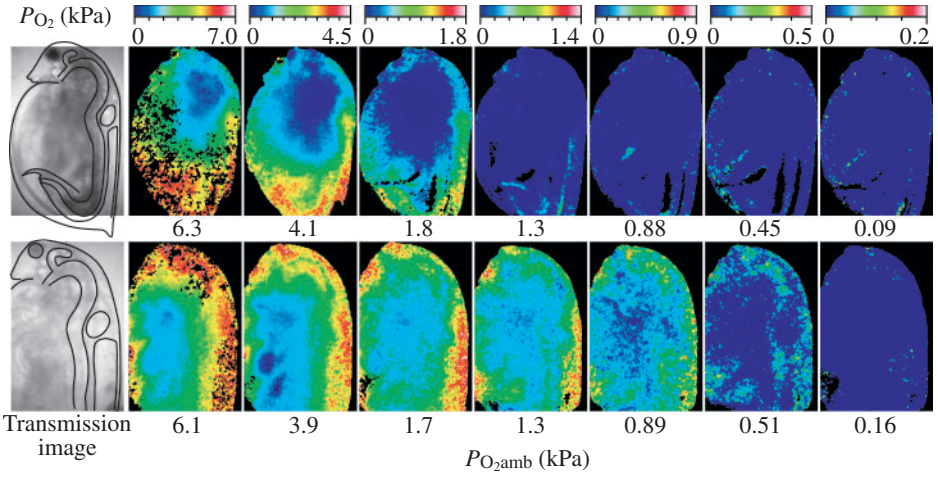

Fig. 6. Two-dimensional distributions of oxygen partial pressure (P_{O_2}) in the haemolymph of a 1.4 mm Hb-poor (top) and a 1.7 mm Hb-rich *Daphnia magna* (bottom), respectively, under different ambient oxygen partial pressures (P_{O_2amb}). The P_{O_2amb} values are indicated below each gallery. Note the different scaling of P_{O_2} in the pseudo-colour images as indicated by the colour bars at the top. During image acquisition, the optical focus was set to the median plane of the animal. For orientation, an image of the animal taken under transmission illumination is shown at the left side of each gallery.

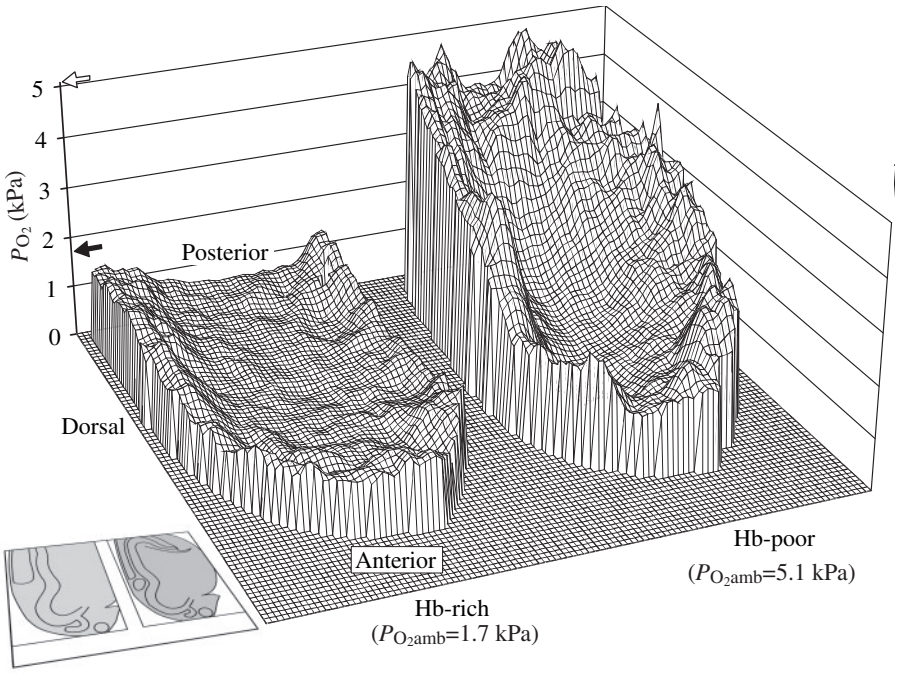

Fig. 7. Oxygen partial pressure (P_{O_2}) distribution in the haemolymph in the median plane of *Daphnia magna*. Left: 1.7 mm Hb-rich animal at an ambient oxygen partial pressure (P_{O2amb}) of 1.7 kPa. Right: 1.4 mm Hb-poor animal at a P_{O2amb} of 5.1 kPa. Note the marked differences in the steepness of the P_{O_2} gradients between both animals. The orientation of the animal with respect to the viewer is indicated by the positional information and by the small sketch in front left.

non-injected animals from the literature. Under normoxic conditions (P_{O2amb}=20 kPa), the small, medium-sized and large Hb-poor animals had mean f_H of 149±47 (N=6), 147±25 (N=4) and 148±36 beats min^{-1} (N=6), respectively. The normoxic f_H of small and medium-sized Hb-rich animals were somewhat lower at 131±5 (N=5) and 136±20 beats min^{-1} (N=7). Neither oxygen acclimation (two-way ANOVA: F=1.26, d.f.=1, P=0.274) nor body size (F=0.01, d.f.=2, P=0.990) had a significant effect on normoxic f_H. In response to a reduction in P_{O2amb} from normoxia (20 kPa) to ~6 kPa hypoxia, all groups showed a compensatory tachycardia followed by a plateau in the range of P_{O2amb} of 1–6 kPa (Fig. 8). The averages of the maximum individual f_H of small, medium-sized and large Hb-poor animals were 293±55, 285±16 and 310±30 beats min^{-1}, respectively. The respective maximum values of Hb-rich animals (small and medium: 226±29 and 246±52 beats min^{-1}) were 14–23% lower than those of Hb-poor animals. The two-way ANOVA showed a significant effect of the acclimation state (F=8.77, d.f.=1, P=0.007) but no significant influence of body size (F=0.53, d.f.=2, P=0.594) on maximum f_H.

Hb concentration in the haemolymph

The haem-based Hb concentrations of small, medium and large Hb-poor animals were 90±8 µmol l^{-1} (N=5), 115±25 µmol l^{-1} (N=6) and 167±38 µmol l^{-1} (N=5), respectively. Hb-rich animals had a five- to sixfold higher concentration with mean values of 450±129 µmol l^{-1} (N=6; small) and 666±132 µmol l^{-1} (N=5; medium).

Influence of Hb concentration and body size on internal P_{O_2}

To compare the internal P_{O_2} of animals of different body size and different Hb concentration, three peripheral positions in the circulatory system of *D. magna* were selected (Fig. 8F): (i) the dorsal lacuna of the trunk, (ii) the carapace lacuna near the median dorsal ridge and (iii) the heart region. Both lacunae conduct the haemolymph to the pericardium, from where it is aspirated by the heart and expelled into the dorsal head region (Pirow et al., 1999b). For small and medium-sized animals, the central body region with the lowest P_{O_2} was additionally analyzed to obtain information on the unloading P_{O_2}.

The highest P_{O_2} values always occurred in the carapace lacuna (Fig. 8; open circles). Since this compartment receives haemolymph that has passed the respiratory surfaces (i.e. the inner walls of the carapace), the P_{O_2} at this position may be regarded as loading P_{O_2}. In all size groups of Hb-poor and Hb-rich animals, the loading P_{O_2} decreased almost linearly with decreasing P_{O2amb} of 1–6 kPa. Moreover, P_{O2amb}–P_{O_2} remained nearly constant, with similar mean values in Hb-poor (small: 0.78, medium: 0.49, large: 0.41 kPa) and Hb-rich animals (small: 0.46, medium: 0.48 kPa). The two-way ANOVA revealed significant effects of oxygen acclimation (F=9.25, d.f.=1, P=0.004) and body size (F=8.40, d.f.=2, P=0.001) on the difference of P_{O2amb}–P_{O_2}.

The dorsal lacuna generally had the lowest P_{O_2} (Fig. 8; open diamonds) in comparison to the other two peripheral positions, with the exception of the small Hb-poor animals (Fig. 8A). At the P_{O2amb} of 6 kPa, the mean P_{O2amb}–P_{O_2} was 3.1–3.7 kPa in the medium and large animals of both acclimation groups, 1.9 kPa in the small Hb-poor animals, and 1.6 kPa in the small Hb-rich animals. Similar to situation in the carapace lacuna, the P_{O_2} in the dorsal lacuna decreased more or less linearly with decreasing P_{O2amb} in the range of 6–2 kPa. However, P_{O2amb}–P_{O_2} did not remain constant but became smaller with decreasing P_{O2amb}. At P_{O2amb}<2 kPa, the P_{O_2} deviated from the trend extrapolated from the linear relationship within the P_{O2amb} of 6–2 kPa.

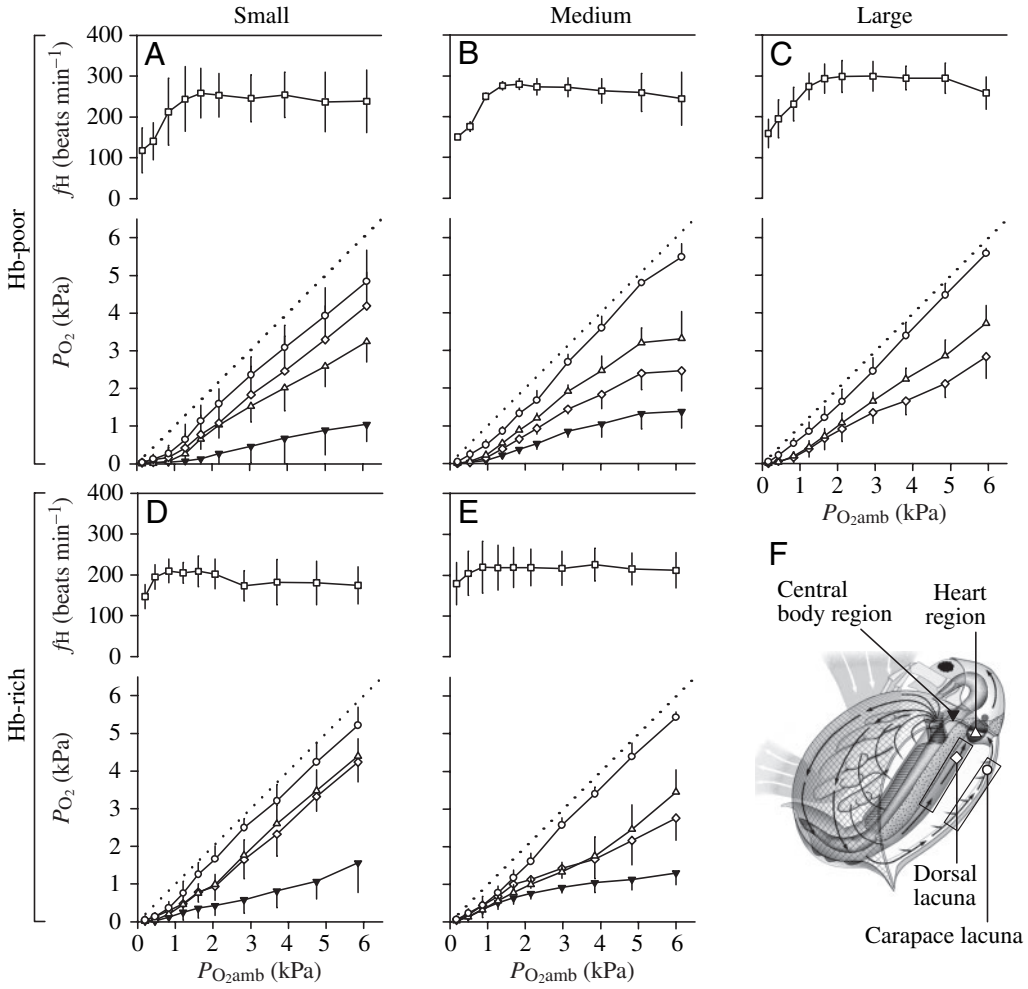

Fig. 8. Responses in internal oxygen partial pressure (P_{O_2}) and heart rate (f_H, open squares) of differently sized (small, medium, large: 1.5±0.12, 2.5±0.3, 3.3±0.13 mm) Hb-poor and Hb-rich *Daphnia magna* to decreasing ambient oxygen partial pressures (P_{O_2amb}). The haemolymph P_{O_2} is given for the carapace lacuna (loading P_{O_2}, open circles), the dorsal lacuna (open diamonds), the heart region (open triangles), and the central body region (unloading P_{O_2}, closed triangles). The dotted lines represent lines of identity where $P_{O_2}=P_{O_2amb}$.

The heart region, which receives haemolymph from the carapace lacuna and the dorsal lacuna, had P_{O_2} values (Fig. 8; open triangles) that were a little higher (Hb-poor animals) than or almost identical (Hb-rich animals) to those in the dorsal lacuna. The only exception were the small-sized Hb-poor animals (Fig. 8A), in which the heart region had a P_{O_2} lower than that at the two other peripheral positions.

In comparison to the three peripheral positions, the unloading P_{O_2} in the central body region (Fig. 8; closed triangles) showed the lowest change per unity change in P_{O_2amb}, indicating a certain degree of oxygen homeostasis. This stabilization was most pronounced in the medium-sized Hb-rich animals, which experienced only a slight decrease in the unloading P_{O_2} from 0.9 to 0.4 kPa upon reduction of P_{O_2amb} from 3 to 1 kPa. Under the same conditions, the unloading P_{O_2} of the medium-sized Hb-poor animals decreased much more markedly from 0.8 to 0.1 kPa. Similar differences in the degree of stabilization were found between the small-sized Hb-rich and Hb-poor animals within the range of P_{O_2amb} of 1–2 kPa.

Discussion

Calibration of Oxyphor R2 in the haemolymph of D. magna

The phosphorescence probe Oxyphor R2 is well suited for measuring oxygen in biological systems in conditions ranging from anoxia to moderate hypoxia (e.g. 70% air saturation; Dunphy et al., 2002). When the probe is bound to albumin, the main constituent of mammalian blood plasma (Urich, 1990), its calibration constants are only slightly affected by pH variations. For 10 µmol l^{-1} solutions of Oxyphor R2 plus 0.15% bovine serum albumin, corresponding to 0.15 g albumin per µmol Oxyphor R2, when pH was increased within the physiological range of pH 7.4–7.8 at 18°C, Dunphy et al. (2002) reported a slight increase of the quenching constant (k_q) from 1576 to 1725 kPa^{-1} s^{-1} and a moderate decrease of the phosphorescence lifetime at zero oxygen tension (τ_0) from 724 to 686 µs. Neglecting such pH-induced variations in k_q and τ_0 would, for example, introduce only a small error of <10% in the calculated oxygen partial pressure (P_{O_2}=7.4–8.2 kPa) for a measured lifetime τ of 70 µs (see Equation 2). Since pH 7.4–7.8 is the physiological value at 20°C in the haemolymph of *D. magna* (Baumeister, 1999) and of other freshwater branchiopod crustaceans (e.g. *Triops cancriformis*, pH 7.52±0.02, N=3; R. Pirow and R. E. Weber, manuscript in preparation), possible variations of haemolymph pH have only minor effects on the characteristics of the oxygen probe. Even if the haemolymph pH should drop to pH 6.4 (k_q=1658 kPa^{-1} s^{-1}, τ_0=790 µs; see Dunphy et al., 2002) under

severe hypoxia as a consequence of activation of anaerobic metabolism, the use of wrong calibration constants such as those for pH 7.4 would give a calculated P_{O_2} of 1.25 kPa instead of 1.24 kPa for a measured τ of 300 µs.

To calibrate Oxyphor R2 in the haemolymph of *D. magna*, a stock solution (pH 7.4) of 360 µmol l^{-1} Oxyphor R2 containing 5.4% bovine serum albumin was injected into the circulatory system, and haemolymph samples were then drawn and measured at 20°C. The concentrations of Oxyphor R2 and albumin resulted in a sufficiently large phosphorescence signal and still permitted the microinjection of the highly viscous stock solution. The proportion of 0.17 g albumin per µmol Oxyphor R2 used in the present study was similar to that used by Dunphy et al. (2002). Despite similar physico–chemical conditions, however, the ranges of our calibration constants (τ_0=451–486 µs; k_q=1364–1535 kPa^{-1} s^{-1}) were somewhat lower than those reported by Dunphy et al. (2002).

Calibration of Oxyphor R2 in Hb-poor and Hb-rich haemolymph at P_{O2amb} within the range 0–4 kPa yielded almost identical τ_0 and k_q values. Only at values of P_{O2amb} >4 kPa did the measured τ of Hb-poor and Hb-rich haemolymph samples differ from each other, suggesting that a variation in Hb concentration might have an influence on the oxygen-dependent properties of the probe at higher P_{O2amb}.

During the experimental series on *Daphnia*, further calibrations in Hb-poor and Hb-rich haemolymph were carried out to obtain parameters for converting *in vivo* lifetime images into P_{O_2} images. The data of these calibration measurements were pooled and yielded a k_q of 1364 kPa^{-1} s^{-1} and a τ_0 of 484 µs for the P_{O2amb} range 0–6 kPa (0–30% air saturation). Since the variability of the measured τ of the different calibrations increased with increasing P_{O2amb} (Fig. 5B), the P_{O_2} determination was more affected by error at higher than at lower P_{O2amb} values, with deviations up to 30%. These deviations resulted from the large variability of individual calibrations and might be caused by variations in the microenvironment of the dye in the circulatory system of animals. For future experiments, separate calibrations for each animal would improve the precision of the measurement.

Influence of the injection procedure on heart beat activity

To measure the internal P_{O_2} optically, the oxygen-sensitive dye had to be introduced into the circulatory system of *D. magna* by microinjection. The injection volume was chosen so as to obtain a sufficiently high phosphorescence signal without affecting the rhythmicity of the heart and the limbs. All injected animals showed the expected compensatory tachycardia (Paul et al., 1997) in response to the reduction in P_{O2amb}, indicating that control of f_H was not affected by the injection procedure. However, the hypoxia-induced maxima of mean f_H (226–310 min^{-1}) of our 1.4–3.5 mm animals appeared to be somewhat lower than those reported for non-injected animals. Reported values obtained under comparable experimental conditions are 342–364 min^{-1} (2.4–2.8 mm animals; Pirow et al., 2001) and 355–379 min^{-1} (2.2–4.0 mm; M. Seidl, R. J. Paul and R. Pirow, manuscript in preparation), respectively. A depression of f_H by the injection procedure therefore cannot be excluded. A plausible explanation for this effect might be the increase in haemolymph viscosity by the introduction of albumin. However, we regard the differences in the maximum f_H between injected and non-injected animals to be of minor consequence for the measured internal P_{O_2} distributions of Hb-poor and Hb-rich animals.

As an animal with a body size in the millimetre range, *D. magna* relies on a mixed diffusive–convective oxygen transport in the circulatory system (Pirow, 2003; Pirow and Buchen, 2004). Consequently, a moderate depression in the convective transport share would be compensated by an increase in the diffusive transport share. This shift from convection to diffusion would steepen internal oxygen gradients (the driving force for diffusion) without affecting the general shape of the oxygen profiles. The effect of a reduced circulatory convection becomes negligible under those ambient oxygen tensions at which Hb is maximally involved in oxygen transport. When Hb is present at high concentration and oxygen is reversibly loaded and unloaded along the steep part of the oxygen equilibrium curve, then Hb can act as an oxygen buffer that damps the effect of fluctuations in perfusion rate on internal P_{O_2}. Finally, further information on non-injected animals is available that supports the validity of the internal P_{O_2} data (see below).

Validation of internal P_{O_2} *data*

Information on internal P_{O_2} values was obtained from the haemolymph spaces in the median plane of the animal. To check the accuracy our internal P_{O_2} data, we used indirect information derived from the oxygenation state of Hb in the heart region of *D. magna*. According to previous studies using medium-sized animals (Pirow et al., 2001; Bäumer et al., 2002), Hb was found to be half-saturated with oxygen at a P_{O2amb} of 2.9–3.2 kPa (Hb-poor animals) and 1.6–2.0 kPa (Hb-rich animals), respectively. Since the oxygen affinities of Hb in whole blood samples of Hb-poor and Hb-rich animals are known (1.0 *vs* 0.5 kPa; Zeis et al., 2003a), it is possible to estimate the difference in oxygen tension between the ambient medium and the heart region (P_{O2amb}–$P_{O2heart}$), and to use this figure for validation purposes. For Hb-poor animals, this estimation yields a difference of (P_{O2amb}–$P_{O2heart}$)=1.9–2.2 kPa, which agrees well with the difference of 1.7–2.0 kPa determined in the present study at P_{O2amb}=2.9–3.2 kPa. The same correspondence with no more than 10% deviation was found in small and large Hb-poor animals (cf. Bäumer et al., 2002). For medium-sized Hb-rich animals, the difference of (P_{O2amb}–$P_{O2heart}$)=1.1–1.5 kPa estimated from the Hb oxygenation state was a little higher than the 0.7–0.9 kPa value determined in the present study. A similar deviation was found for small Hb-rich animals (cf. Bäumer et al., 2002). This discrepancy is, however, not particularly surprising since the half-saturation oxygen tension of Hb in our Hb-rich animals could have been a little higher than 0.5 kPa, because this value was the lowest one

reported by Zeis et al. (2003a) for whole blood of hypoxia-acclimated Hb-rich animals.

The shape of the two-dimensional oxygen profiles

Imaging of internal P_{O_2} distribution in small-sized animals of *D. magna* revealed interesting information concerning the internal pathway of oxygen. In Hb-poor animals, there was a steep overall anterior to posterior gradient, containing a localized region of much lower P_{O_2} (Figs 6, top, 7). The lowest values occurred in the centre of the anterior half of the animal, a region densely packed with the large, active muscles of the second antennae and the mandibles. A localized oxygen sink in this region suggests that these body structures are the first ones to suffer from an undersupply of oxygen in situations of progressive environmental hypoxia. Indeed these tissues, including the bases of the limb muscles, proved to be sensitive, early indicators (*via* NADH fluorescence) of the incipient impediment of tissue oxygen supply in *D. magna* (Pirow et al., 2001). The global shape of the two-dimensional oxygen profiles is well in line with model predictions (Pirow and Buchen, 2004) as well as with results of an experimental study that used Hb as an internal oxygen probe (Pirow et al., 1999b), and the general description of the internal pathway for oxygen in *D. magna* is corroborated by the present study.

When flowing through the limbs and subsequently along the inner walls of the carapace valves, the haemolymph takes up oxygen from the ambient medium (see Fig. 8F). During this oxygenation process, haemolymph moves in the posterior direction, which explains the high P_{O_2} values found in the posterior body region of the animals (Fig. 6, top). The oxygenated haemolymph in the carapace eventually reaches the median dorsal ridge of the carapace (carapace lacuna in Fig. 8F) before returning to the pericardium. Along the way to the heart, the haemolymph may lose oxygen by centripetal diffusion, which explains the posterior–anterior gradient in P_{O_2} (Fig. 7, Hb-poor case). In the pericardium, the haemolymph from the carapace lacuna becomes mixed with that from the dorsal lacuna. The dorsal lacuna receives haemolymph that has passed the intestinal lacuna, the fifth limb pair, and the post-abdomen. From the pericardium, the haemolymph is aspirated by the heart and expelled into the dorsal head region, from where it moves to the central nervous system before entering the ventral and intestinal lacunae of the trunk.

Keeping the haemolymph and medium flow pattern (Fig. 8F) in mind, the formation of a global gradient directed posterior-to-anterior can be easily explained by (i) uptake of oxygen into the haemolymph that moves along the ventral body side in a posterior direction, and (ii) centripetally directed diffusive loss of oxygen from the haemolymph that flows along the dorsal side in an anterior direction.

The sixfold higher Hb concentration in Hb-rich animals resulted in a flattening of internal oxygen profiles under hypoxic conditions (Figs 6, bottom, 7). The large anterior–posterior gradient, characteristic of Hb-poor animals, disappeared and the high P_{O2} values extended into the head region. This pattern with high oxygenation values in the rostral region has already been reported (Pirow et al., 1999b) and shows that the head region, with its sensory and central nervous structures, still receives an adequate supply when ambient oxygen becomes less available. This observation indicates that Hb-rich animals have a striking physiological advantage over Hb-poor animals. The increase in Hb concentration also caused a shift of the low-oxygen zone from the anterior to the central body region (Fig. 6, bottom). Both these observations, the smoothing of oxygen gradients and the positional shift of the low-oxygen zone, indicate that the extra Hb buffers the haemolymph P_{O_2} and enhances the convective oxygen transport in the circulatory system. The presence of steep P_{O_2}

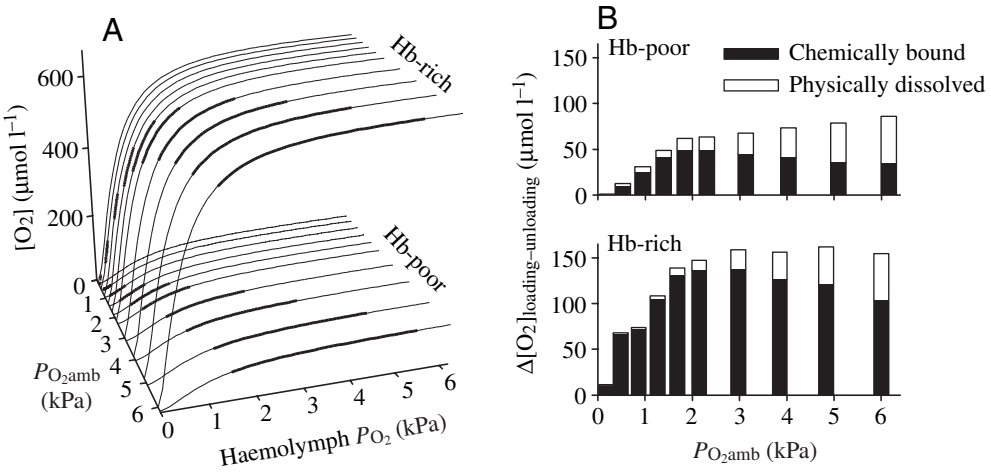

Fig. 9. Involvement of Hb in circulatory oxygen transport. (A) The range between the loading and unloading oxygen partial pressure (P_{O_2}; bold solid lines) of medium-sized Hb-poor and Hb-rich animals under different ambient oxygen tensions (P_{O_2amb}) was mapped onto the oxygen equilibrium curve of Hb (thin solid lines). The ordinate shows the concentration of chemically bound oxygen ($[O_2]$), which is the product of the fractional oxygen saturation of Hb (S) and haem concentration ([Haem]; Hb-poor: 115 µmol l^{-1}, Hb-rich: 666 µmol l^{-1}). Oxygen equilibrium curves (S *vs.* haemolymph P_{O_2}) were calculated according to the Hill equation assuming a cooperativity coefficient of 1.6 (Kobayashi et al., 1988) and half-saturation oxygen tensions of 1.0 kPa (Hb-poor) and 0.5 kPa (Hb-poor; Zeis et al., 2003a), respectively. (B) Differences between the loading and unloading $[O_2]$ in relation to P_{O_2amb} for Hb-poor (top) and Hb-poor animals (bottom). Black and white bars refer to the physically dissolved and chemically bound portions of transported oxygen, respectively. A value of 12.3 µmol l^{-1} kPa^{-1} was assumed as solubility coefficient for oxygen in haemolymph (Pirow and Buchen, 2004).

gradients in Hb-poor animals, by contrast, suggests that diffusion is more important for internal transport processes.

Importance of body size and Hb concentration on internal P_{O_2}

Based on the quantitative information available for the three peripheral and one central body region (Fig. 8F), we found no obvious influence of body size on internal P_{O_2} except in small Hb-poor animals. In these animals, the P_{O_2} in the carapace lacuna (i.e. the loading P_{O_2}; Fig. 8F) was 0.8 kPa below the P_{O2amb}, whereas in all other groups, the difference between P_{O2amb} and loading P_{O_2} was only 0.4–0.5 kPa. Moreover, of the three peripheral positions analyzed, the heart region generally assumed an intermediate P_{O_2} value, except again in small Hb-poor animals, where the heart P_{O_2} was lowest (Fig. 8A). These distinguishing characteristics of the small Hb-poor animals suggest a greater diffusive loss of oxygen from the haemolymph to the tissues when flowing (i) from the respiratory surfaces to the carapace lacuna, as well as (ii) from the carapace lacuna and the dorsal lacuna to the heart. Internal oxygen transport in the smaller Hb-poor animals therefore appears to be effected more by diffusion than in larger Hb-poor counterparts. Short transport distances from the peripheral to central body regions, in combination with the internal oxygen gradient, are prerequisites for a high diffusive flux and may explain this effect of body size. However, we cannot exclude the possibility that the injection of the viscous dye solution overproportionally slowed circulation in the smallest animals, thereby contributing to the shift from convective to diffusive oxygen transport. The absence of this body-size/injection effect within the Hb-rich animals can be explained by the presence of a greater concentration of circulating Hb, which stabilizes internal P_{O_2} and smooths oxygen gradients.

This smoothing and stabilizing effect of Hb was most striking in medium-sized Hb-rich animals, in which the P_{O_2} values of the monitored body regions converged with a progressive reduction of P_{O2amb} from 3 to 1 kPa (Fig. 8E). Under these conditions, the unloading P_{O_2} decreased only slightly from 0.4–0.9 kPa, which indicated an oxygen homeostasis in the central body region. The P_{O_2} at this position was well above zero required to drive the diffusion of oxygen from the haemolymph into the tissues. Medium-sized Hb-poor animals, by contrast, experienced a much stronger decrease of the unloading P_{O_2} from 0.8 to 0.1 kPa (Fig. 8B) under the same ambient conditions. The strong decrease of unloading P_{O_2} in these animals very likely reflects the inability of the circulatory system to sustain the oxygen supply to the centrally located tissues. This suggestion is corroborated by respiration measurements, which showed that 2.5 mm Hb-poor animals of *D. magna* are unable to sustain their oxygen uptake rate at a P_{O2amb} lower than 4 kPa at 20°C (Kobayashi and Hoshi, 1984). The shut-down of aerobic metabolism might also explain the strong convergence of the monitored P_{O_2} values that occurred in all groups at P_{O2amb} <1 kPa.

Direct measurement of internal P_{O_2} is ideal for quantitative assessment of the contribution of Hb to circulatory oxygen transport. Since most experimental data and model calculations are available for *D. magna* 2.5 mm long (for references, see Pirow, 2003; Pirow and Buchen, 2004), we restricted our assessment to medium-sized animals. By making reasonable assumptions about the oxygen binding characteristics of Hb, it was possible to determine from the loading and unloading P_{O_2} curves (Fig. 8B,E) those parts of the oxygen equilibrium curve that were used for reversible oxygen binding under different P_{O2amb} conditions (Fig. 9A). This analysis indicated that Hb-rich animals reversibly load and unload oxygen over a progressively smaller part of the oxygen equilibrium curve with decreasing P_{O2amb}. A similar tendency was present in Hb-poor animals.

Information on the operation range of the oxygen equilibrium curve was further employed to determine the difference between the loading and unloading oxygen concentration ($\Delta[O_2]$) in the haemolymph (Fig. 9B). The fact that $\Delta[O_2]$ was about twice as high in Hb-rich animals compared to Hb-poor animals strongly points towards a greater contribution of convection to circulatory oxygen transport. To estimate this convective contribution, we initially ignored the role of diffusion and assumed that all oxygen is transported by circulatory convection. If this assumption is correct, then the Fick principle of convection should yield an oxygen transport rate (= stroke volume × heart rate × $\Delta[O_2]$) that is equal to the oxygen consumption rate of the animal. From the *BL* of Hb-poor and Hb-rich animals (2.6 *vs* 2.7 mm), the stroke volume (8.2 *vs* 9.0 nl) and the oxygen consumption rate (24 *vs* 26 nmol h^{-1}) were calculated according to Bäumer et al. (2002). For maximum $\Delta[O_2]$ (86 *vs* 162 μmol l^{-1}; Fig. 9B) and maximum heart rates (285 *vs* 246 min^{-1}; Fig. 8B,E), we obtained convective transport rates that accounted for 50% and 85% of the oxygen consumption rates of Hb-poor and Hb-rich animals, respectively. While these results showed the assumption of an exclusive convective transport to be invalid, they can nevertheless be regarded as a measure of relative contribution of convection to circulatory oxygen transport. The remaining 50% and 15% are then accounted for by a diffusional transport occurring in parallel to convection.

List of symbols

BL	body length
I_0	phosphorescence intensity (arbitrary units) at time t=0
I_t	phosphorescence intensity (arbitrary units) at time t
f_H	heart rate (min^{-1})
k_q	quenching constant (kPa^{-1} s^{-1})
P_{O_2}	oxygen partial pressure (kPa)
P_{O2amb}	oxygen partial pressure in the ambient medium (kPa)
$P_{O2heart}$	oxygen partial pressure in the heart region (kPa)
S	fractional oxygen saturation of haemoglobin
t	time (s)
Z	integrated phosphorescence intensity (arbitrary units)

t_d	delay time (s)
x,y	pixel coordinates
τ_0	phosphorescence lifetime (s) at zero oxygen tension
τ	phosphorescence lifetime (s)
ΔT	gating pulse duration (s)

The technical assistance of Ina Buchen is gratefully acknowledged. Supported by the Deutsche Forschungsgemeinschaft (Pa 308/7-1).

References

Baumeister, U. (1999). Säure-Basen-Regulation und Respiration bei Zooplankton-Organismen. Diploma thesis, University of Münster, Germany.

Bäumer, C. (2001). Optische Analyse des zirkulatorischen Sauerstofftransports im großen Wasserfloh, *Daphnia magna*. PhD thesis, University of Münster, Germany.

Bäumer, C., Pirow, R. and Paul, R. J. (2002). Circulatory oxygen transport in the water flea *Daphnia magna*. *J. Comp. Physiol. B* **172**, 275-285.

Becher, B. (2002). Untersuchungen zur hypoxie-induzierten Hämoglobin-Synthese des großen Wasserflohs *Daphnia magna*. PhD thesis, University of Münster, Germany.

Burggren, W. and Fritsche, R. (1995). Cardiovascular measurements in animals in the milligram range. *Brazil. J. Med. Biol. Res.* **28**, 1291-1305.

Colmorgen, M. and Paul, R. J. (1995). Imaging of physiological functions in transparent animals (*Agonus cataphractus*, *Daphnia magna*, *Pholcus phalangioides*) by video microscopy and digital image processing. *Comp. Biochem. Physiol. A* **111**, 583-595.

Dunphy, I., Vinogradov, S. A. and Wilson, D. F. (2002). Oxyphor R2 and G2: phosphors for measuring oxygen by oxygen-dependent quenching of phosphorescence. *Anal. Biochem.* **310**, 191-198.

Elendt, B.-P. and Bias, W.-R. (1990). Trace nutrient deficiency in *Daphnia magna* cultured in standard medium for toxicity testing. Effects of the optimization of culture conditions on life history parameters of *D. magna*. *Wat. Res. Biol.* **245**, 1157-1167.

Fritzsche, H. (1917). Studien über Schwankungen des osmotischen Druckes der Körperflüssigkeiten bei *Daphnia magna*. *Int. Rev. ges. Hydrob. Hydrog.* **8**, 22-80.

Green, J. (1956). Variation in the haemoglobin content of *Daphnia*. *Proc. R. Soc. B* **145**, 214-232.

Hoshi, T. and Yahagi, N. (1975). Studies on physiology and ecology of plankton. XXIX. *In vivo* equilibrium of oxygen with blood haemoglobin of *Daphnia magna*. *Sci. Rep. Niigata Univ. Ser. D (Biol.)* **12**, 1-7.

Kimura, S., Tokishita, S., Ohta, T., Kobayashi, M. and Yamagata, H. (1999). Heterogeneity and differential expression under hypoxia of two-domain hemoglobin chains in the water flea, *Daphnia magna*. *J. Biol. Chem.* **274**, 10649-10653.

Kobayashi, M. (1982). Influence of body size on haemoglobin concentration and resistance to oxygen deficiency in *Daphnia magna*. *Comp. Biochem. Physiol.* A **72**, 599-602.

Kobayashi, M. (1983). Estimation of the haemolymph volume in *Daphnia magna* by haemoglobin determination. *Comp. Biochem. Physiol. A* **76**, 803-805.

Kobayashi, M. and Hoshi, T. (1982). Relationship between the hemoglobin concentration of *Daphnia magna* and the ambient oxygen concentration. *Comp. Biochem. Physiol. A* **72**, 247-249.

Kobayashi, M. and Hoshi, T. (1984). Analysis of respiratory role of haemoglobin in *Daphnia magna*. *Zool. Sci.* **1**, 524-532.

Kobayashi, M. and Tanaka, Y. (1991). Oxygen-transporting function of hemoglobin in *Daphnia magna*. *Can. J. Zool.* **69**, 2968-2972.

Kobayashi, M., Fujiki, M. and Suzuki, T. (1988). Variation in and oxygen-binding properties of *Daphnia magna* hemoglobin. *Physiol. Zool.* **61**, 415-419.

Lo, L. W., Vinogradov, S. A., Koch, C. J. and Wilson, D. F. (1997). A new, water soluble, phosphor for oxygen measurements *in vivo*. *Adv. Exp. Med. Biol.* **428**, 651-656.

Paul, R. J., Colmorgen, M., Hüller, S., Tyroller, F. and Zinkler, D. (1997). Circulation and respiratory control in millimetre-sized animals (*Daphnia magna*, *Folsomia candida*) studied by optical methods. *J. Comp. Physiol. B* **167**, 399-408.

Paul, R. J., Colmorgen, M., Pirow, R., Chen, Y. H. and Tsai, M. C. (1998). Systemic and metabolic responses in *Daphnia magna* to anoxia. *Comp. Biochem. Physiol. A* **120**, 519-530.

Pawlowski, M. and Wilson, D. F. (1994). Imaging oxygen pressure in tissue in vivo by phosphorescence decay. *Adv. Exp. Med. Biol.* **361**, 83-93.

Piiper, J. (1982). Respiratory gas exchange at lungs, gills and tissues – mechanisms and adjustments. *J. Exp. Biol.* **100**, 5-22.

Pirow, R. (2003). The contribution of hemoglobin to oxygen transport in the microcrustacean *Daphnia magna* – A conceptual approach. *Adv. Exp. Med. Biol.* **510**, 101-107.

Pirow, R. and Buchen, I. (2004). The dichotomous oxyregulatory behaviour of the planktonic crustacean *Daphnia magna*. *J. Exp. Biol.* **207**, 683-696.

Pirow, R., Wollinger, F. and Paul, R. J. (1999a). The importance of the feeding current for oxygen uptake in the water flea *Daphnia magna*. *J. Exp. Biol.* **202**, 553-562.

Pirow, R., Wollinger, F. and Paul, R. J. (1999b). The sites of respiratory gas exchange in the planktonic crustacean *Daphnia magna*: An *in vivo* study employing blood haemoglobin as an internal oxygen probe. *J. Exp. Biol.* **202**, 3089-3099.

Pirow, R., Bäumer, C. and Paul, R. J. (2001). Benefits of haemoglobin in the cladoceran crustacean *Daphnia magna*. *J. Exp. Biol.* **204**, 3425-3441.

Schwerte, T. and Fritsche, R. (2003). Understanding cardiovascular physiology in zebrafish and *Xenopus* larvae: the use of microtechniques. *Comp. Biochem. Physiol. A* **135**, 131-145.

Seidl, M., Pirow, R. and Paul, R. J. (2002). Water fleas (*Daphnia magna*) provide a separate ventilatory mechanism for their brood. *Zoology* **105**, 15-23.

Shelton, G. (1992). Model applications in respiratory physiology. In *Oxygen Transport in Biological Systems*, vol. 51, *SEB Seminar Series* (ed. S. Egginton and H. F. Ross), pp. 1-44. Cambridge: Cambridge University Press.

Urich, K. (1990). *Vergleichende Biochemie der Tiere*. Stuttgart, New York: Gustav Fischer Verlag.

Vanderkooi, J. M. and Wilson, D. F. (1986). A new method for measuring oxygen in biological tissues. *Adv. Exp. Med. Biol.* **200**, 189-193.

Vinogradov, S. A. and Wilson, D. F. (1994). Phosphorescence lifetime analysis with a quadratic C-programming algorithm for determining quencher distributions in heterogeneous systems. *Biophys. J.* **67**, 2048-2059.

Weber, R. E. and Vinogradov, S. N. (2001). Nonvertebrate hemoglobins: Functions and molecular adaptations. *Physiol. Rev.* **81**, 569-628.

Weibel, E. R. (1984). *The Pathway for Oxygen*. Cambridge, MA: Harvard University Press.

Weibel, E. R. (1979). *Stereological Methods*, vol. 1. London, UK: Academic Press.

Weibel, E. R. (1980). *Stereological Methods*, vol. 2. London, UK: Academic Press.

Zar, J. H. (1999). *Biostatistical Analysis*. Upper Saddle River, NJ: Prentice Hall.

Zeis, B., Becher, B., Goldmann, T., Clark, R., Vollmer, E., Bölke, B., Bredebusch, I., Lamkemeyer, T., Pinkhaus, O., Pirow, R. and Paul, R. J. (2003a). Differential haemoglobin gene expression in the crustacean *Daphnia magna* exposed to different oxygen partial pressures. *Biol. Chem.* **384**, 1133-1145.

Zeis, B., Becher, B., Lamkemeyer, T., Rolf, S., Pirow, R. and Paul, R. J. (2003b). The process of hypoxic induction of *Daphnia magna* hemoglobin: subunit composition and functional properties. *Comp. Biochem. Physiol. B* **134**, 243-252.